Journal of Contemporary Technology and Applied Engineering (JCTAE), **2**(1), 2023, 1-11

DOI: 10.21608/JCTAE.2022.160463.1011 Published by: *Faculty of Engineering, Kafrelsheikh University*

EFFECTS OF SURFACE INJECTION OR EJECTION AT VARIOUS ANGLES ON THE HEAT TRANSFER AND FLOW FIELD IN A RECTANGULAR CHANNEL

Received: 03-09-2022
Accepted: 07-09-2022

A.S. Abdullah[a], A.M. El-Zahaby[a], M.K. Bassiouny[b], A. Khalil[a], E.A. El-Shenawy[a], Z.M. Omara[c,*]

[a] *Department of Mechanical Power Engineering, Faculty of Engineering, Tanta University, Egypt*

[b] *Department of Mechanical Power Engineering, Faculty of Engineering, Menoufia University, Shebin El-Kom, Egypt*

[c] *Mechanical Engineering Department, Faculty of Engineering, Kafrelsheikh University, Kafrelsheikh 33516, Egypt*

[*] corresponding author: Z. M. Omara (zm_omara@eng.kfs.edu.eg)

ABSTRACT. With surface ejection or injection occurring at various angles in a rectangular channel, the subject of forced convection heat transfer and fluid flow characteristics is investigated numerically. Thus, the numerical solution of the two-dimensional set of governing differential equations of continuity, momentum, and energy in Cartesian coordinates. At the duct input, it is presumed that the flow will be steady with constant characteristics and uniform velocity and temperature profiles. The Gauss-Siedel iterative method is used to solve algebraic system of equations. Utilizing a bundled "ANSYS" based on the "SIMPLE" technique, computational fluid dynamics is applied. Investigations are conducted into how temperature fields and flow patterns are affected by Reynolds number, injection or ejection angle, mass flow rate, and other variables. The relevant factors in the current study range from 4000 to 120000 for the Reynolds number, from 0.0 to 4 for the blowing ratio, and from 0° to 180° for the injection or ejection angles. The findings demonstrate that under constant injection angles, the blowing ratio increases along with the Nusselt number and friction coefficient ratios. For injection situations at 90° with a Reynolds number, the Nusselt number enhancement is greater. At various injection angle values, a comparison between injection and ejection is made. The generated theoretical results are evaluated against published experimental and experimental data. The comparisons demonstrate good agreement with an average relative error of 4.6%.

KEYWORDS: Turbulent flow; secondary flow; heat transfer; injection or ejection surface; flow characteristics.

NOMENCLATURE

C_p	Specific heat at const. press., J/kg.K
C_f	Local skin friction coefficient
$\overline{C_f}$	Average skin friction coefficient
d	Injection tube diameter, m
g	Gravitational acceleration, m/s^2
H	Duct height, m
h	Heat transfer coefficient, W/m^{2}K
HR	Height ratio, H/d
M	Blowing ratio, $\varrho_{inj}\, U_{inj} / \varrho_\infty\, U_\infty$
Nu	Local Nusselt number, h d /k
$\overline{Nu}$	Average Nusselt number
Pr	Prandtl number, $\mu\, C_p/k$
Q	Rate of Heat Transfer, W
Q_o	Rate of heat transfer without injection
Re	Reynolds number , $U_{inlet}\, d/\nu$
S	Distance from center-to-center of injection, m
SR	Span ratio, S/d
T	Mean temperature, K
u	Velocity component in x direction, m/s
v	Velocity component in y direction, m/s
w	Velocity component in z direction, m/s
Subscripts	
f	Fluid
inj	Injection
o	Without Injection

w	Wall
Greek symbols	
Δ	Difference
μ	Dynamic viscosity, kg/m.s
ν	Kinematic viscosity, m^2/s
η	Film cooling effectiveness, $(T_w-T_{fw}/ T_w-T_{inj})$
∞	Free stream
Γ	Diffusion coefficient, Γ= μ/Pr
Φ	Angle of injection or ejection
λ	Thermal conductivity, W/m.K

1. INTRODUCTION

In many engineering applications, the channel flow that results in fluid mass withdrawal at the flow boundaries is encountered. Such flows can be seen, for instance, in channels with porous walls that are chosen at random. The forced-convection condensation in a tube application is another often used example. In this scenario, a vapor moves through the core as condensed liquid flows in an annular layer next to the tube's cooled wall. It is also used to lower the wall temperature of combustion chambers in rocket motors and to cool reentry spacecraft through the injection of coolant through porous walls. Other technical problem areas where permeable surfaces are useful include wave attenuation in fluidic circuits, cooling of turbine blades, and jet engine noise reduction. Other technical issues that permeable surfaces have found widespread use in include wave attenuation in fluidic circuits, cooling of turbine blades, gaseous diffusion processes, and jet engine noise reduction.

Kinney et al. [1] use numerical methods to simulate turbulent flow, heat transfer, and mass transfer in a tube with surface suction. Suction or blowing at the boundary significantly affects all transfer coefficients, including friction, heat transfer, and mass transfer, according to data for other forms of turbulent flows, particularly exterior flows. Eriksen et al. [2] study experimentally heat transmission and film cooling by injection through inclined circular tubes. Both a single hole and a row of holes with three-diameter spacing and an angle of 35 degrees to the main flow are used to inject air. Experimental research on the impact of vortices with various circulations on heat transmission and injectant downstream of a row of film-cooling holes in a turbulent boundary layer was conducted by Ligrani et al. [3]. Along with heat transfer measurements and mean velocity surveys, mean temperature results that demonstrated how injectant is distorted and then redistorted by vortices were also provided. Analytical research on a steam injection into a sluggish water flow through porous media was conducted by Chung et al. [4]. For both water and steam flow, the continuity, momentum, and energy equations were solved under interface circumstances.

Ligrani et al. explored the effects of a single row and two staggered rows of holes with 6d and 3d spanwise spacing, respectively, on film cooling through experiments in their publications [5] and [6]. This arrangement places holes 3d apart in the spanwise direction, with their inclinations to the test surface being 30 and 35 degrees. The adiabatic film cooling efficiency had Spanwise-averaged values that were best at a blowing ratio of 0.5 and dropped as blowing ratio increased. Experimental research on the impact of flow turbulence on film cooling effectiveness was done by Lebedev et al. [7].

Experimental research on the impact of injection hole length on film cooling with bulk flow pulsations was conducted by Seo et al. [8] Krogstad et al. [9] 's investigation of some localized injection effects on boundary layer turbulence structure. Several tests have been described by Burd and Simon [10], Burd et al. [11], Oke, et al. [12], and Oke et al. [13] for various injection strategies upstream of a nozzle guide vane with a contoured end wall. Coolant was injected from an interrupted, flush slot that was slanted at 45° slightly upstream of their vanes in the investigations published by Burd and Simon [10], Burd et al. [11], and Oke, et al. [12]. Similar to other researchers, they discovered that under low slot flow circumstances, the majority of the slot coolant was directed toward the suction side. But their observations showed that the coverage between the airfoils improved when they increased the slot flow percentage to 3.2% of the exit flow. The investigation by Oke et al. [13] used a double row of film cooling holes that were 45° angled with respect to the surface and aligned with the flow direction, yet it still managed to maintain almost the same ideal 3% bleed flow as their earlier studies. They discovered that the single slot performed better thermally than the jets because the single slot produced less mixing and the jets rose off the surface more.

Film cooling flow effects on post-combustor trace chemistry were described by Thomas et al. [14]. The reasons are the drop of the gas stagnation temperature at the exit of the combustion chamber to a lower value at the exit of nozzle guiding vane and the loss of total pressure resulting from the mixing of the cooling air with the mainstream. El-Emam et al [15] .'s theoretical and experimental studies of the two-dimensional jet's cross-flow flow characteristics. The concentration distribution was achieved experimentally using image digitization technology and a slit jet with a width of 1

mm. A two-dimensional model was used to theoretically calculate the velocity distribution. Jets in cross flow at various velocity ratios were the subject of an experimental correlation. Ming et al. [16] used a numerical method to investigate the impact of hole form on the efficiency of film cooling on flat plates, incorporating internal impingement cooling chamber. The main-flow, injection tubes, impingement chamber, and supply plenum sections of a flat, three-dimensional discrete-hole film cooling geometry were all included in the numerical technique. The effects of the blowing ratio and the shape of the holes were investigated, along with the distributions of the flow field and the effectiveness of the adiabatic film cooling across a flat plate with two rows of injection holes in a staggered-hole pattern.

A power-law fluid food's heat transfer and fluid flow during the heating process through an unequal channel with non-uniform injection/suction were explored numerically in Reference [17]. Filtration and permeation are used in many industrial applications. Permeation happens when fluids pass through porous media. For instance, Hassan et al. [18]'s investigation of nanofluid flow over a wavy surface in a porous medium illustrates this. Bhatti et al. [20] proposed a mathematical model to mimic the flow of an electrically conducting Prandtl fluid through a homogeneous porous media in a non-uniform annulus. In order to understand the function of porosity in the HT, Alamri et al. [19] examined a Poiseuille nanofluid in a channel with Stefan blowing. Ref. [22] conducted an analysis of a nanofluid in a vertical channel with a porous material under the influence of entropy production. Shirvan et al. [21] studied the natural convection HT of a fluid in an inclined porous solar cavity receiver under the influence of surface radiation. Fetecau et al. [23] determined the solutions to the second Stokes problem pertaining to fluid motion across a moving plate while taking porous influences into consideration. Ref. [24] looked at the mass and HT of a two-phase fluid passing through a so-called Darcy-Brinkman-Forchheimer porous medium.

Considering the results of previous investigations which did not cover all possible geometrical and operating parameters the need of more investigations arises. Therefore, the problem of flow through channels with surface ejection or injection at different angles is theoretically investigated in this study. Both the hydrodynamic and the thermal boundary layers at the channel wall can be controlled by removing or injecting fluid through the wall. This results in an enhancement of the heat transfer coefficient.

2. MATHEMATICAL MODELING

2.1. INTRODUCTION

A rectangular channel with surface ejection or injection is considered. The air flow in the channel is assumed to be turbulent and the k-ε model technique is applied in this case. After setting up the governing equations, which describe the channel air flow, a numerical model is used to convert them into a set of algebraic equations. Then, a computational fluid dynamics method using a packaged " ANSYS" is used based on the "SIMPLE" technique introduced by Patanker [25].

2.2. THE MATHEMATICAL MODEL AND METHOD OF SOLUTION

The physical model, which describes the case of study, is illustrated in Fig. (1). the supply, injected flow is distributed along the top wall, therefore, the flow can be approximated by two-dimensional flow (2D) in the x-y plan. The ejection and injection holes are shown in the figure. The duct is 700 mm long and 70 mm height. The bottom wall is adiabatic insulated and the top wall is heated at constant heat flux (q_w = const.). The injection or ejection angle (Φ) varies from 0^o to 180^o. The flow is assumed steady incompressible and the properties of air are assumed to be constant except density in the buoyancy term. The used coordinate system is shown in Fig. 1. The effects of gravity force and heat dissipation are neglected. Moreover, uniform velocity and temperature profiles at the inlet cross section of the duct are considered.

Cartesian coordinate system (x, y, and z) is used to express the flow governing equations for a channel cross-section. Solving the flow describing equations, velocity and temperature distributions throughout the flow field can be determined and hence, the physical quantities of the flow, such as heat transfer coefficient and Nusselt number, can be calculated. The solid boundaries except the top wall are assumed to be insulated.

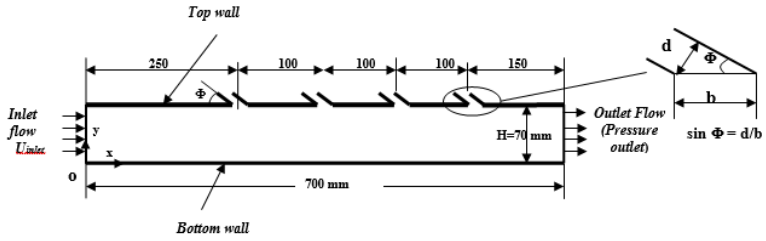

Fig. 1. The physical model.

2.3. TURBULENCE MODEL

The task of turbulence model is to express the fluctuation components in the governing equations by a set of auxiliary equations containing time-mean quantities of flow. These auxiliary equations permit the closure of the time mean dependent variables in the transport equations which are usually called "closure equations". The k-ε model is used and the fluctuating properties are represented by three new turbulent properties: turbulent eddy viscosity, turbulent kinetic energy, and turbulent dissipation rate (ε). The turbulence viscosity is directly related to the turbulence kinetic energy and its dissipation rate as:

$$\mu_t = C_\mu \rho \frac{k^2}{\varepsilon} \quad (1)$$

Where, ϱ is the fluid density, C_μ the turbulence kinetic energy and its dissipation rate are represented by transport equations.

By considering that the air flow is incompressible, steady flow, and variable density, the time derivatives are canceled in the governing equations. The continuity equation is:

$$\frac{\partial(\rho u)}{\partial x} + \frac{\partial(\rho v)}{\partial y} + \frac{\partial(\rho w)}{\partial z} = 0$$

The momentum equations in x, y, z directions are:

$$\frac{\partial(\rho u^2)}{\partial x} + \frac{\partial(\rho uv)}{\partial y} + \frac{\partial(\rho uw)}{\partial z} = -\frac{\partial p}{\partial x} + \frac{\partial}{\partial x}\left(\mu_e \frac{\partial u}{\partial x}\right) + \frac{\partial}{\partial y}\left(\mu_e \frac{\partial u}{\partial y}\right) + \frac{\partial}{\partial z}\left(\mu_e \frac{\partial u}{\partial z}\right) - \frac{2}{3}\frac{\partial}{\partial x}(\rho k)$$

$$\frac{\partial(\rho uv)}{\partial x} + \frac{\partial(\rho v^2)}{\partial y} + \frac{\partial(\rho vw)}{\partial z} = -\frac{\partial p}{\partial y} + \frac{\partial}{\partial x}\left(\mu_e \frac{\partial v}{\partial x}\right) + \frac{\partial}{\partial y}\left(\mu_e \frac{\partial v}{\partial y}\right) + \frac{\partial}{\partial z}\left(\mu_e \frac{\partial v}{\partial z}\right) - \frac{2}{3}\frac{\partial}{\partial y}(\rho k) + g(\rho - \rho_o)$$

$$\frac{\partial(\rho uw)}{\partial x} + \frac{\partial(\rho vw)}{\partial y} + \frac{\partial(\rho w^2)}{\partial z} = -\frac{\partial p}{\partial z} + \frac{\partial}{\partial x}\left(\mu_e \frac{\partial w}{\partial x}\right) + \frac{\partial}{\partial y}\left(\mu_e \frac{\partial w}{\partial y}\right) + \frac{\partial}{\partial z}\left(\mu_e \frac{\partial w}{\partial z}\right) - \frac{2}{3}\frac{\partial}{\partial z}(\rho k)$$

The energy equation is:

$$\frac{\partial(\rho uT)}{\partial x} + \frac{\partial(\rho vT)}{\partial y} + \frac{\partial(\rho wT)}{\partial z} = \frac{\partial}{\partial x}\left(\Gamma_e \frac{\partial T}{\partial x}\right) + \frac{\partial}{\partial y}\left(\Gamma_e \frac{\partial T}{\partial y}\right) + \frac{\partial}{\partial z}\left(\Gamma_e \frac{\partial T}{\partial z}\right) + S_T \quad (6)$$

where:

ϱ_o density at reference temperature T_o, μ_e effective viscosity, $\mu_e = \mu + \mu_t$ and

Γ_e effective diffusion factor, $\Gamma_e = \Gamma + \Gamma_t = \Gamma + (\mu_t/Pr_t)$.

The k and ε-transport equations developed by the turbulent model are:

$$\frac{\partial(\rho uk)}{\partial x} + \frac{\partial(\rho vk)}{\partial y} + \frac{\partial(\rho wk)}{\partial z} = \frac{\partial}{\partial x}\left(\Gamma_k \frac{\partial k}{\partial x}\right) + \frac{\partial}{\partial y}\left(\Gamma_k \frac{\partial k}{\partial y}\right) + \frac{\partial}{\partial z}\left(\Gamma_k \frac{\partial k}{\partial z}\right) + \mu_t\left\{2\left[\left(\frac{\partial u}{\partial x}\right)^2 + \left(\frac{\partial v}{\partial y}\right)^2 + \left(\frac{\partial w}{\partial z}\right)^2\right] + \left(\frac{\partial u}{\partial y} + \frac{\partial v}{\partial x}\right)^2 + \left(\frac{\partial u}{\partial z} + \frac{\partial w}{\partial x}\right)^2 + \left(\frac{\partial w}{\partial y} + \frac{\partial v}{\partial z}\right)^2\right\} - \rho\varepsilon + \beta g \Gamma_t \frac{\partial T}{\partial y}$$

$$\frac{\partial(\rho u\varepsilon)}{\partial x} + \frac{\partial(\rho v\varepsilon)}{\partial y} + \frac{\partial(\rho w\varepsilon)}{\partial z} = \frac{\partial}{\partial x}\left(\Gamma_k \frac{\partial \varepsilon}{\partial x}\right) + \frac{\partial}{\partial y}\left(\Gamma_k \frac{\partial \varepsilon}{\partial y}\right) + \frac{\partial}{\partial z}\left(\Gamma_k \frac{\partial \varepsilon}{\partial z}\right) + C_1 \frac{\varepsilon}{k}\mu_t\left\{2\left[\left(\frac{\partial u}{\partial x}\right)^2 + \left(\frac{\partial v}{\partial y}\right)^2 + \left(\frac{\partial w}{\partial z}\right)^2\right] + \left(\frac{\partial u}{\partial y} + \frac{\partial v}{\partial x}\right)^2 + \left(\frac{\partial u}{\partial z} + \frac{\partial w}{\partial x}\right)^2 + \left(\frac{\partial w}{\partial y} + \frac{\partial v}{\partial z}\right)^2\right\} - C_2\rho\frac{\varepsilon^2}{k} + C_1\beta g \frac{\varepsilon}{k}\Gamma_t \frac{\partial T}{\partial y}$$

Where: $\Gamma_k = \frac{\mu + \mu_t}{Pr_k}$ and $\Gamma_\varepsilon = \frac{\mu + \mu_t}{Pr_\varepsilon}$

The k-ε model equations (1), (6), (7) and (8) contain six constants namely C_μ, C_1, C_2, Pr_t, Pr_k, and Pr_ε. The standard values of these constants are presented in Table (1).

Finally, for steady incompressible turbulent flow in a duct, whereby all fluctuating variables are assigned time-mean equivalents through the turbulent model, the momentum and energy equations may be rewritten as:

$$\frac{\partial}{\partial x_i}(\rho u\phi) = \frac{\partial}{\partial x_i}\left(\Gamma_\varphi \frac{\partial \phi}{\partial x_i}\right) + S_\varphi \quad (9)$$

Where the dependent variable φ represents the velocity components u, v, w, and T and the scales of turbulence used in the turbulence model Γ_φ and S_φ represent the diffusion and source terms.

Table 1. Standard values of k-ε model constants for air.

Cμ	C1	C2	Prt	Prk	Prε
0.09	1.44	1.92	1	1.3	0.9

2.4. PROBLEM DESCRIPTION

The flow passage is modeled as 70×700 mm with a long width. The air at inlet and outlet flow has ambient pressure. Top wall contains a set of injection holes arranged in such a way that the distance between each two sets is the same and the first hole is located at 250 mm from inlet section. The lengths of the injection hole in the wall are variables according to the injection angle. A top wall represents the representation of a simple cooling flat surface. These duct constitutions are chosen to simplify the domain, so it can be easily considered as a two-dimensional domain.

2.5. NUMERICAL GRIDS

The domain is represented in the used code by a two-dimensional model. The domain is divided into rectangular cells. The height is divided into 28 cells while the length is divided into 280 cells (N_x= 28, N_y= 280). Some modifications are done to the grid to ensure the accurate computations in the zones where properties sharp variation is expected.

2.6. BOUNDARY CONDITIONS

Boundary conditions are required along all the domain boundaries for all dependent variables in order to complete system of equations. For a number of years, investigations in duct flow by Computational fluid dynamics (CFD) have been carried out using simplified boundary conditions and mainly focusing on the internal flow. Boundary conditions are given in Table (2).

3. Results and Discussions

The results are obtained in terms of the operating and geometric parameters. The operating parameters are Reynolds number (Re) and the blowing ratio (M). The geometric parameter is the injection angle (Φ), height ratio (HR) and span ratio (SR).

3.1. Validity of the Present Model

The numerical results of the current study are compared with the relevant experimental data obtained by Dittus-Boelter correlation (Nu = 0.023 *Re0.8 * Pr0.4), as shown in Fig. 2, in order to assess the model's viability. It is evident that the results of the Dittus-Boelter Correlation and those from the current study are in good agreement, with a relative error having an average of 6.2%.

Table 2. Boundary conditions

Boundary		Type and Location, mm	Variables		
			T, K	U, m/s	V, m/s
Inlet flow		Velocity inlet {X = 0, 0 ≤ y ≤ 70}	300	0.8 → 25	0
Injections	Angle Φ ◦	Velocity inlet y = 70	300	0.04CosΦ → 100CosΦ	-0.04 SinΦ → -100 Sin Φ
Walls	Top wall	Wall y = 70	q=const.	0	0
	Bottom wall	Wall y = 0	Insulated wall	0	0
Out flow		($P_{out} = P_{atm}$) {X=700, 0 ≤ y ≤ 70}	-	-	-

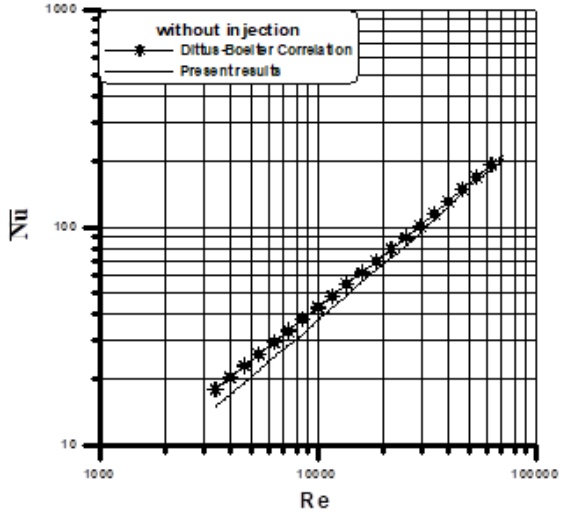

Fig. 2. *Without injection, comparison between the present Nusselt number and Dittus-Boelter correlation.*

3.2. Variation of Local Parameters with and without Injection

Fig. 3 illustrates the variation of flow parameters inside the duct without injection at Re=4000. The fluid temperature at the top surface is shown in Fig.3a. The fluid surface at the top is heated and its temperature increases along the surface. It is clear that the slop of the curve is high at the inlet while it decreases to small value after a position of 0.2 m from the inlet. The velocity of the fluid decreases steeply, where friction constrains the velocity. The skin friction is proportional to the velocity and by increasing the temperature of fluid at the wall, the surface Nusselt number decreases which depends on the heat transfer coefficient. The effect of injection is indicated in Fig.4, where the local of both Nusselt number and skin friction coefficient increases at the beginning of each injection, due to the decrease of the temperature and the increase in velocity respectively.

Fig. 5 shows the effect of blowing ratio M on the pair of rotating vortices. It may be noticed that, in case of low blowing ratios, the core of eddies appears near the wall and it moves far from the wall by higher blowing ratios. The magnitude of the velocity increases from inside to outside eddies, so the enhancement of heat transfer occurs

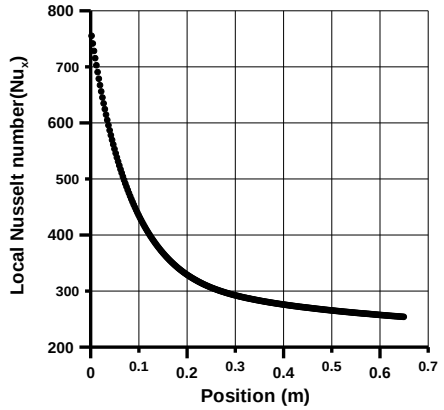

(a) Local Nusselt number

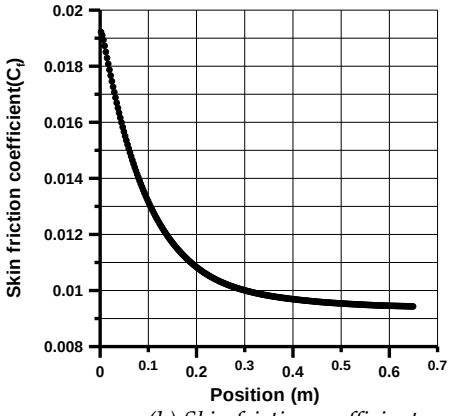

(b) Skin friction coefficient

Fig. 3. Variation of the parameters for flow inside the duct without injection at Re = 4000

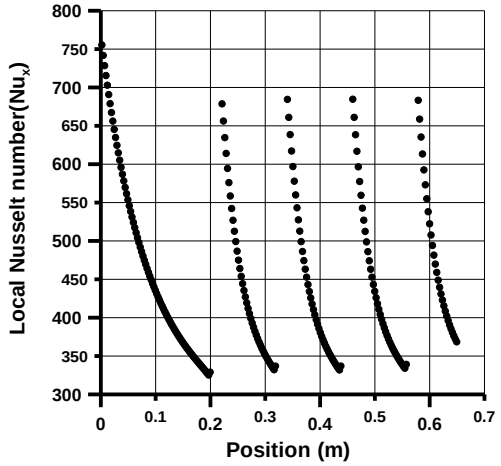

(a) Local Nusselt number

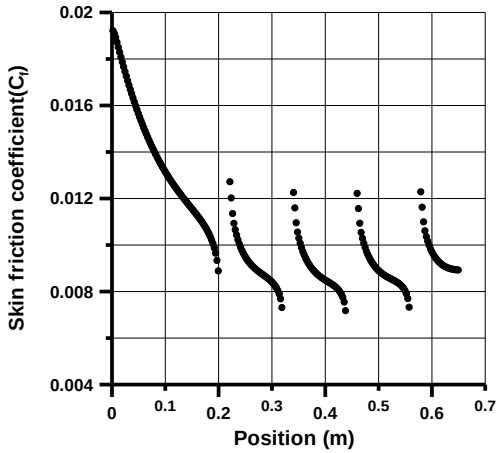

(b) Skin friction coefficient

Fig. 4. Variation of the parameters for flow inside the duct with injection at Re = 4000, Φ = 15° and M = 0.5.

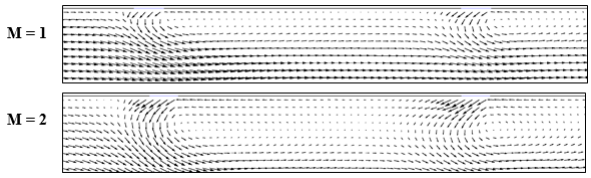

Fig. 5. Effect of blowing ratio (M) on the velocity vector at injection angle 150°

3.3. Effect of Reynolds Number

Fig. 6 show the change of flow and heat transfer parameters with Reynolds number Re at different values of the injection angles Φ for M= 2. The results are plotted for the Reynolds number ranged from 4000 to 120000. It is clearly seen that by injection or ejection the effectiveness and average Nusselt number ratio increase for all values of Re. In the dominated flow Re> 30000, the effectiveness increases slightly with increasing Reynolds number while for Re< 10000, the effectiveness increases dramatically with increasing of Reynolds number, where the temperature of the fluid neighboring the wall is increasing slowly for higher Re. Effect of Reynolds number on average Nusselt number ratio for different injection angles is shown in Fig. 8a. The increased values of the average Nusselt number may return to the high turbulence levels near the edges of jets, which occur at Φ > 90° as shown in Fig. 8a and Fig.10a. For injection angles < 90°, the turbulence levels due to interaction between them is low and the average Nusselt number ratio is approximately constant for all values of Reynolds number. At Re≈8000, the separation of the fluid from the wall occurs, so the drop of the turbulence kinetic energy, the friction coefficient and Nusselt number occur for both injection and ejection. Figure 10-b shows no variation of the average turbulence kinetic energy for Re> 30000, so in this range the effectiveness, the average Nusselt number and the average friction coefficient are changing slowly. The plots indicate that the increase of the average Nusselt number up to 2.5 times is reported at Φ=165° and M= 2, in case of injection

3.4. Effect of Blowing Ratio

In Fig.7, the cross-stream average Nusselt number ratio is plotted against the blowing rate for different injection and ejection angles. The Reynolds number is Re=64000. For injection case, with a large injection angle Φ=165°, the average Nusselt number ratio increases as the blowing ratios increases. With a small injection angle Φ≤ 90°, the average Nusselt number ratio decreases from blowing rates M=0.05 to minimum value at M=0.5, after that the Nusselt number ratio is returning to increase. In addition, the average friction coefficient ratio lowers to values less than those without blowing where the ratio $\overline{C_f}/\overline{C_{f_o}}$ is less than unity.

Many processes acting in the near wall flow disturbed by film cooling injection may partially compensate each other and in some cases, it remains yet unknown what influence prevails. The influence of some parameters is obvious and confirmed under certain circumstances: high blowing rates cause violent mixing and interaction of the jets with high turbulence levels increasing the heat transfer rate. High heat transfer coefficients for shallow injection and low heat transfer rates for normal injection are in agreement with the effects in thin respectively thick boundary layers. The phenomenon of lowering the heat transfer by small blowing rates particularly just downstream of the injection may be due to smoothing the wall. In this case the small normal velocity components of the almost laminar jets may lift off the sublayer whereas the effect of increasing the turbulence level by mixing and interaction is lower with small blowing rates. Up to now these investigations were restricted to experimental work. In ejection case this phenomenon appears, where the average Nusselt number ratio increases with M until reaches a maximum value at 0.7≤M≤1 for all ejection angles. After that the average Nusselt number decreases to a minimum value at

M=1.5 for most ejection angles, where $\overline{Nu}/\overline{Nu}_o$ =1.3, the friction coefficient decreases for the same reasons. An enhancement in maximum average Nusselt number for ejection at angle 15° is up to 68%, while the maximum average ratio $\overline{Nu}/\overline{Nu}_o$ up to 400% is reported in at angle 165°.

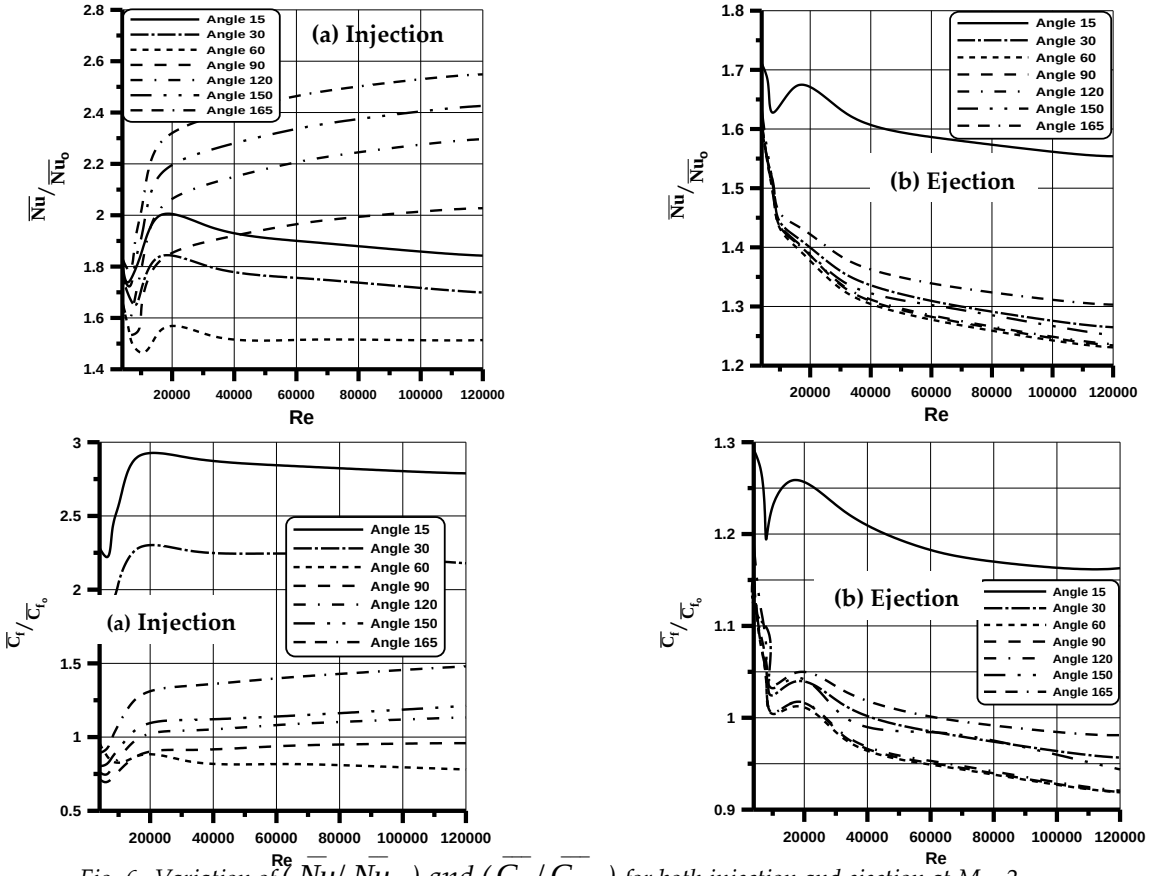

Fig. 6. Variation of ($\overline{Nu}/\overline{Nu}_o$) and ($\overline{C}_f/\overline{C}_{f_o}$) for both injection and ejection at M = 2.

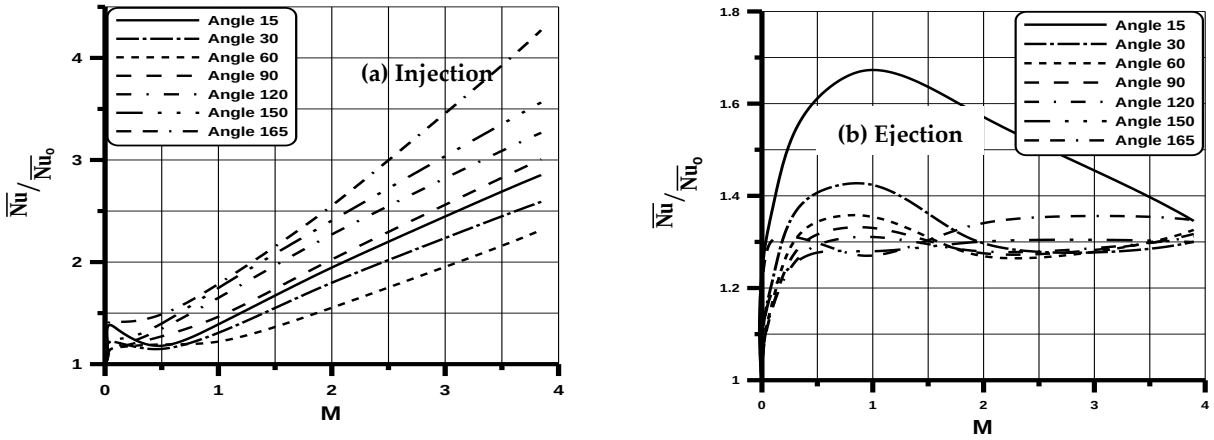

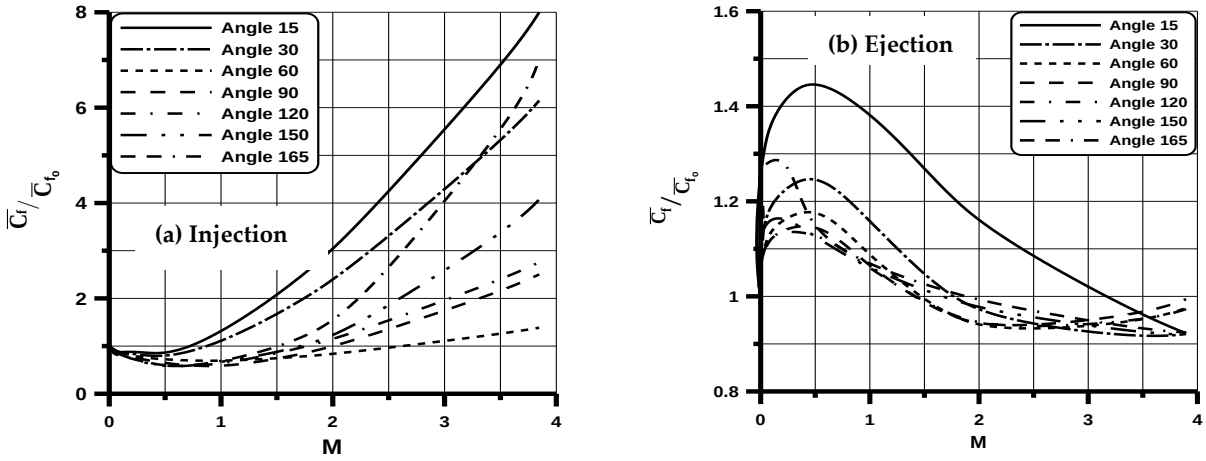

Fig. 7. *Variation of* $(\overline{Nu}/\overline{Nu}_o)$ *and* $(\overline{C}_f/\overline{C}_{f_o})$ *with blowing ratio (M) for both injection and ejection at Re = 64000.*

3.5. EFFECT OF ANGLE OF INJECTION OR EJECTION

Fig. 8 indicates the variation of average Nusselt number ratio and the average friction coefficient ratio with the injection angle (Φ) for both injection and ejection at *Re* = 64000. Heat transfer increases from the low value at the zero and 180° injection angles to reach a peak at the two angles 15° and 165° for all blowing ratios. The highest value of average Nusselt number ratio for injection is 2.44 occurs at Φ=165° and a blowing ratio equals 2, while the corresponding value in case of ejection occurs at 15° is 1.55.

The friction coefficient at angle = 15° is the highest while it drops to minimum at the angle 60° for injection. The highest value of the average turbulent kinetic energy ratio occurs at 165°. In case of ejection, the curves start to increase to a maximum value and then decrease to a minimum value. They repeat themselves as sine or cosine waves. The curves, which represent M=0.05 are somewhat symmetrical.

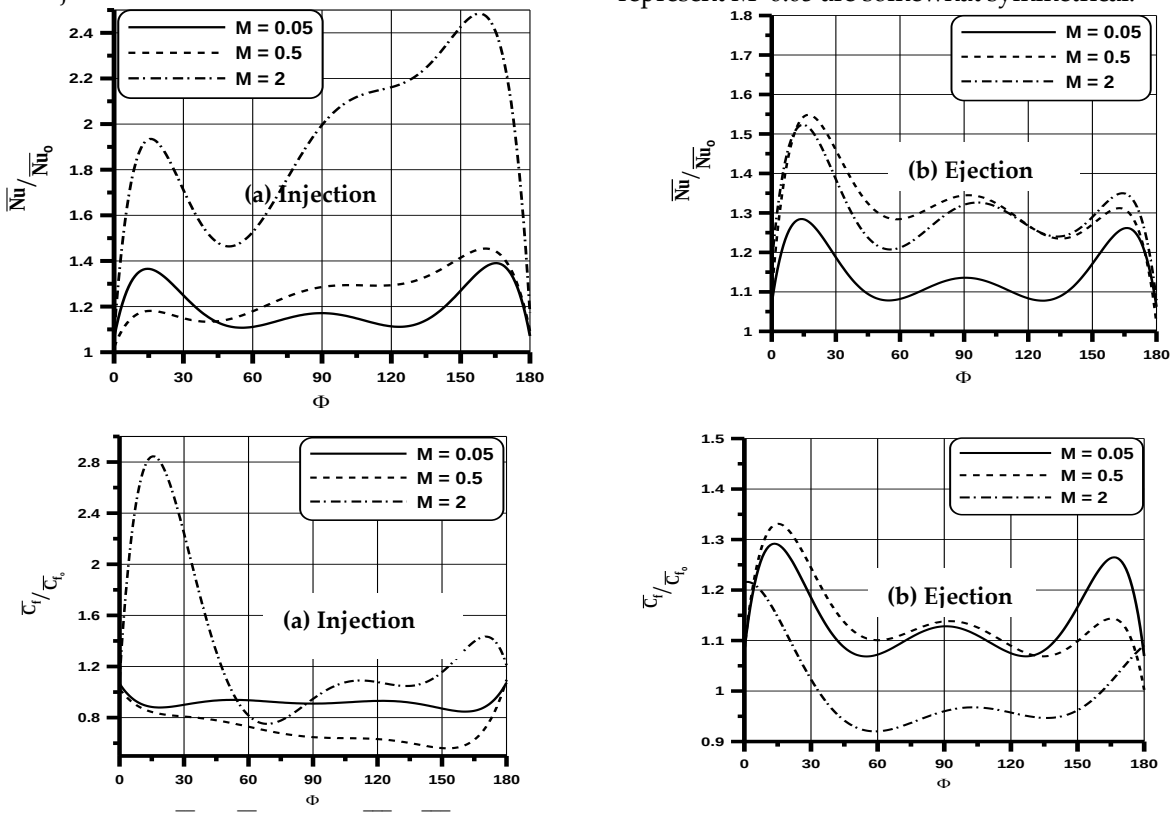

Fig. 8. Variation of $(\overline{Nu}/\overline{Nu}_o)$ ***and*** $(\overline{C}_f/\overline{C}_{f_o})$ *with injection angle (**Φ**) for both injection and ejection at Re = 64000.*

3.6. EFFECT OF HEIGHT AND SPAN RATIOS

Fig. 9 represent the variation of the average Nusselt number ratio with height ratio (HR) and the span ratio (SR) for injection at *Re* = 10000. The average Nusselt number ratio increases with increasing HR for high blowing ratios (M=2, but no variation in the enhancement of heat transfer with the height ratio for lower blowing ratio (M=0.5). The average Nusselt number ratio decreases with increasing the span ratio for all blowing ratios, as indicated in Fig.

3.7. COMPARISON BETWEEN EJECTION AND INJECTION

Fig. 10 indicates a comparison between injection and ejection for average Nusselt number ratio against the blowing ratio at different Reynolds numbers. The curves show that the enhancement of heat transfer in case of injection is more than that in case of ejection at angles 120° and 150° for all values of the blowing ratio, while for angles 30° and 60° it is true only at low values of M. For higher values of M, we have the other way round. Also, figure explains a comparison between injection and ejection for average skin friction coefficient ratio against the blowing ratio at different Reynolds numbers. The trend of the curves takes almost the same trend of Nusselt number curves except that the average skin friction coefficient ratio for ejection is higher than that for injection in a wide range of blowing ratio specially at low Reynolds numbers.

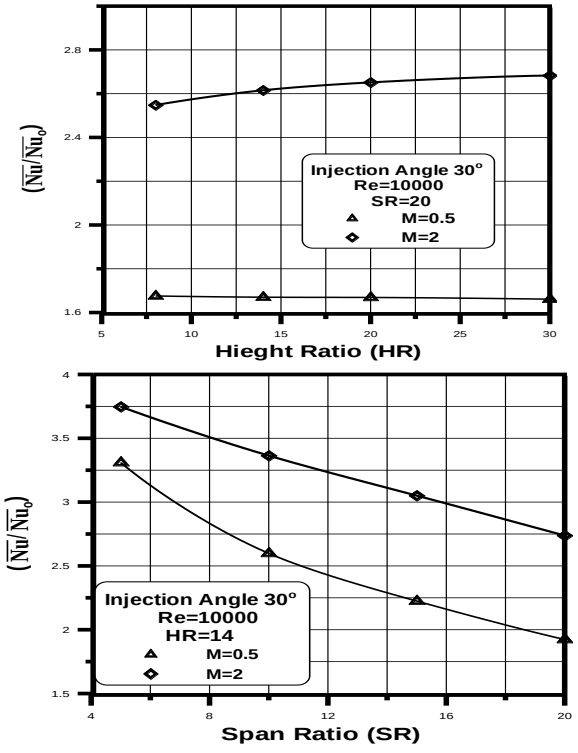

Fig. 9. Variation of $\overline{Nu}/\overline{Nu}_o$ *with height ratio (HR) and span ratio (SR) for injection at Re = 10000.*

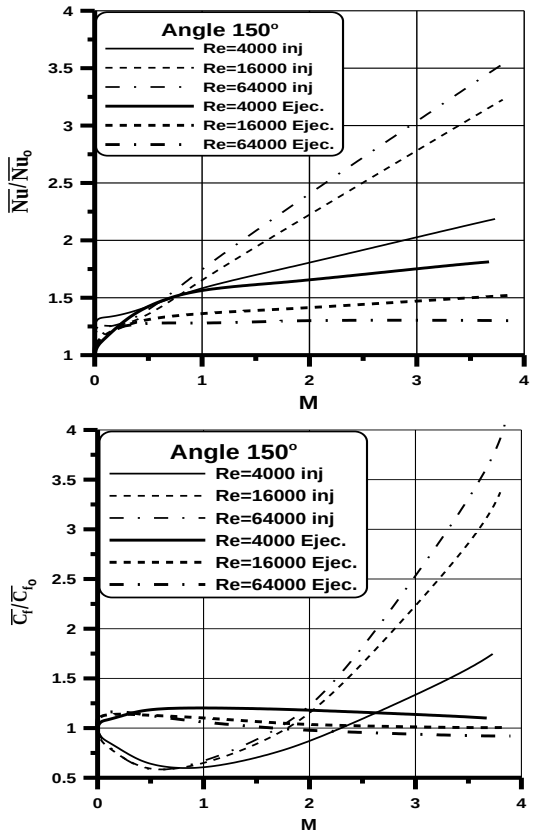

Fig. 10. Comparison between injection and ejection for average Nusselt number ratio and average skin friction coefficient ratio at different Reynolds numbers.

4. CONCLUSIONS

In this work, the 2-D steady incompressible turbulent flow in rectangular duct with surface injection and ejection are solved numerically. The solutions are reached for different values of injection angle (Φ), blowing ratio ($0.0 \le M \le 4$) and Re between 4000 and 120000. The results show that for injection the average of both Nusselt number ratio and skin friction coefficient ratio increase with increasing Re for injection angles $\Phi > 90°$,and vice versa $\Phi < 90°$ at a fixed value of M. The foregoing mentioned parameters decrease for all angles Φ in ejection cases. Due to the separation of flow at the wall especially for lower values of Re, a sudden drop in both the average Nusselt number ratio and skin friction coefficient ratio occurs. The length of the recirculation zone and the separation were increase with increasing the blowing ratio at a fixed value of Φ. On the other hand, the maximum enhancement in heat transfer occurs at two angles 15° and 165°, where the local velocity and the turbulence kinetic energy are highest at these angles. In addition, the average Nusselt number ratio decreases with increase the height ratio (HR) of the channel at lower blowing ratio and $\overline{Nu}/\overline{Nu}_o$ increase with HR at high values of M. On the other hand, the average Nusselt number ratio decreases with increasing the span ratio (SR) for all values of M. The

ejection is preferred at lower values of Re and M with respect to injection. A good agreement between the results of Eriksen [2] and those obtained from the present work is clear whereas the average deviation is 2.1%. The comparisons show a good agreement.

REFERENCES

[1] Kinney, R. b., and Sparrow, E. M., "Turbulent Flow, Heat Transfer, and Mass Transfer in a Tube with Surface Suction", Journal of heat transfer, Feb. 1970, pp. 117-125.

[2] Eriksen, v. L., Goldstein, R. J., "Heat Transfer and Film Cooling Following Injection through Inclined Circular Tubes", Journal of heat transfer, May. 1974, pp. 239-245.

[3] Ligrani, P. M., and Subramanian, C. S., Craig, D. W., and Kaisuwan, P., " Effects of Vortices with Different Circulations on Heat Transfer and Injectant Downstream of a Row of Film-Cooling Holes in a Turbulent Boundary Layer ", Journal of heat transfer, Feb. 1991, vol. 113, pp. 79-90.

[4] Chung, M., and Catton, I., "Steam Injection into a Slow Water Flow through Porous Media", Journal of heat transfer, Aug. 1993, vol. 115, pp. 734-120.

[5] Ligrani, P. M., Wigle, J. M., Cirello, S., and Jackson, S. W., " Film-Cooling From Holes With Compound Angle Orientations: Part 1-Results Downstream of two Staggered Rows of Holes With 3d Spanwise Spacing", Journal of heat transfer, May. 1994, vol. 116, pp. 341-352.

[6] Ligrani, P. M., Wigle, J. M., Jackson, S. W., "Film-Cooling From Holes with Compound Angle Orientations: Part 2-Results Downstream of a Single Row of Holes With 6d Spanwise Spacing", Journal of heat transfer, May. 1994, vol. 116, pp. 353-362.

[7] Lebedev, V. P., Lemanov, V. V., Misyura, S. Ya., and Terekhov, V. I., " Effects of Flow turbulence on Film Cooling Efficiency ", Int. J. of Heat and Mass Transfer, vol. 38,No. 11, pp. 2117-2125, 1995.

[8] Seo, H. J., Lee, J. S., and Ligrani, P. M., "The Effect of Injection Hole Length on Film Cooling with Bulk Flow Pulsations", Int. J. of Heat and Mass Transfer, vol. 41, pp. 3515-3528, 1998.

[9] Per-Age Krogstad, and Anatoli Kourakine, " Some Effects of Localized Injection on the Turbulence Structure in a Boundary Layer ", physics of fluids, Nov. 2000, vol. 12, No. 11, pp. 2990-2999.

[10] Burd, S. W. and Simon, T. W., "Effects of Slot Bleed Injection over a Contoured Endwall on Nozzle Guide Vane Cooling Performance: Part I: Flow Field Measurements", 2000-GT-199.

[11] Burd, S. W., Satterness, C. J., and Simon, T. W., "Effects of Slot Bleed Injection over a Contoured Endwall on Nozzle Guide Vane Cooling Performance: Part II Thermal Measurements", 2000-GT-200.

[12] Oke, R., Simon, T., Burd, S. W., Vahlberg, R., "Measurements in a Turbine Cascade Over a Contoured Endwall: Discrete Hole Injection of Bleed Flow", 2000-GT-214.

[13] Oke, R., Simon, T., Shih, T. Zhu, B., Lin, Y. L., Chyu, M. "Measurements Over a Film-Cooled, Contoured Endwall with Various Coolant Injection Rates", 2001-GT-140.

[14] Thomas Wey and Liu, N. S., "Film Cooling Flow Effects on Post-Combustor Trace Chemistry", 16th Int. Symp. on Air Breathing Engines, ISABE-2003 –No. 1090.

[15] S. H. El-Emam, H. Mansour, A. R. Abdel-Rahim, and M. M. El-khayat, " Flow Characteristics of Two-Dimensional Jet in Crossflow", 4th IEC - Faculty of Eng.- Mansoura Univ. - Egypt-2004 – pp. M-471-478.

[16] Jr-Ming Miao, and Chen-Yuan Wu, "Numerical approach to hole shape effect on film cooling effectiveness over flat plate including internal impingement cooling chamber", International journal of heat and Mass Transfer -2006, vol. 49, pp. 919- 938.

[17] Botong Li, Yikai Yang, Xuehui Chen, "A power-law liquid food flowing through an uneven channel with non-uniform suction/injection", International Journal of Heat and Mass Transfer, May. 2019, vol. 144, pp.118639.

[18] M. Hassan, M. Marin, A. Alsharif, R. Ellahi, Convection heat transfer flow of nanofluid in a porous medium over wavy surface, Phys. Lett. A 382 (2018) 2749–2753.

[19] M.M. Bhatti, A. Zeeshan, R. Ellahi, O. Anwar Bég, A. Kadir, Effects of coagulation on the two phase peristaltic pumping of magnetized Prandtl biofluid through an endoscopic annular geometry containing a porous medium, Chin. J. Phys. 58 (2019) 222–234.

[20] S.Z. Alamri, R. Ellahi, N. Shehzad, A. Zeeshan, Convective radiative plane Poiseuille flow of nanofluid through porous medium with slip: an application of Stefan blowing, J. Mol. Liq. 273 (2019) 292–304.

[21] R. Ellahi, M. Raza, N.S. Akbar, Study of peristaltic flow of nanofluid with entropy generation in a porous medium, J. Porous Media 20 (5) (2017) 461–478.

[22] K.M. Shirvan, M. Mamourian, S. Mirzakhanlari, R. Ellahi, K. Vafai, Numerical investigation and sensitivity analysis of effective parameters on combined heat transfer performance in a porous

solar cavity receiver by response surface methodology, Int. J. Heat Mass Transf. 105 (2017) 811–825.

[23] C. Fetecau, R. Ellahi, M. Khan, N.A. Shah, Combine porous and magnetic effects on some fundamental motions of Newtonian fluids over an infinite plate, J. Porous Media 21 (7) (2018) 589–605.

[24] M.M. Bhatti, A. Zeeshan, R. Ellahi, G.C. Shit, Mathematical modeling of heat and mass transfer effects on MHD peristaltic propulsion of two-phase flow through a Darcy-Brinkman-Forchheimer porous medium, Adv. Powder Technol. 29 (2018) 1189–1197.

[25] Fluent Inc., Version 6.0, 2002 (Fluent Inc: New Hampshire).